Eur. Phys. J. D **16**, 225–228 (2001)

THE EUROPEAN PHYSICAL JOURNAL D

EDP Sciences

Pure and Sb-doped SnO_2 nanoparticles studied by photoelectron spectroscopy

C. McGinley[1,a], S. Al Moussalami[1], M. Riedler[2], M. Pflughoefft[3], H. Borchert[3], M. Haase[3], A.R.B. de Castro[4], H. Weller[3], and T. Möller[1]

[1] HASYLAB/DESY, Notkestrasse 85, D-22603 Hamburg, Germany
[2] II. Institut für Experimentalphysik, Universität Hamburg, Luruper Chaussee 149, D-22761 Hamburg
[3] Institut für Physikalische Chemie, Universität Hamburg, D-22761 Hamburg, Germany
[4] Laboratorio National de Luz Sincrotron, Campinas 13081-90, Brazil

Received 30 November 2000

Abstract. We describe photoemission results from pure and Sb-doped SnO_2 nanoparticles deposited on gold substrates. Photoelectron spectra with synchrotron radiation were recorded for Sn 3d, Sb 3d and O 1s core levels and valence bands in the 500-1200 eV energy range. For pure SnO_2 nanoparticles the surface is terminated by an oxygen rich layer with no obvious surface environment for Sn. When doped n-type with 9.1% or 16.7% Sb, dopant atoms are concentrated near the surface of the nanoparticles. The valence state of the dopant atoms is predominantly Sb^V. Plasmon satellite features are also observed in core level photoemission spectra and their intensity relative to the main peak increases with increasing photon energy.

PACS. 61.46.+w Nanoscale materials: clusters, nanoparticles, nanotubes, and nanocrystals – 79.60.-i Photoemission and photoelectron spectra – 61.72.Ww Doping and impurity implantation in other materials

1 Introduction

Semiconductor nanoparticles show a distinct size dependence with regard to various physical properties [1,2]. Some of these concern electronic structure so there is an inevitable interest in doping these systems in order to understand size confinement in unison with variation of carrier concentration. Shim and Guyot-Sionnest have recently achieved this for II-VI nanoparticles [3].

Colloidal chemical preparation methods have been successful in preparing n-type SnO_2 by the introduction of 2-20% Sb in the particles and subsequent annealing to 500 °C [4]. Thin films of these particles show an electrochromic effect, *i.e.* a reversible colour change is caused by the injection of electrons through the sample [5,6]. It is interesting therefore to investigate how the Sb is distributed throughout the nanoparticles, to elucidate its valence state, Sb^{III} or Sb^V for instance, and to clarify which surface and bulk chemical bonds are present. Photoelectron Spectroscopy (PES) with synchrotron radiation is the technique we have used to answer these questions in order to develop a description of the electronic characteristics of doped semiconductor nanoparticles.

[a] e-mail: mcginley@mail.desy.de

2 Experiment

Photoemission Experiments were performed at the undulator beamline BW3 at Hasylab/DESY, where the SX700 monochromator provides photons in the 100-1200 eV range. Measurements were made using a new UHV experimental chamber which includes a fast entry load lock for sample transfer and an Omicron EA125 hemispherical energy analyser (HEA) for acquiring the photoemission spectra. By varying the photon energy we could vary the sampling depth in the experiment. A combined photon and electron experimental resolution of 240 meV was used in recording core level spectra. These were subsequently fitted to the minimum number of Voigt lineshape functions after subtraction of a polynomial background. Fitting was by TCFIT which uses Levenberg-Marquadt and Simplex optimisation routines.

The preparation method of the Sb-doped SnO_2 nanoparticles has been described elsewhere [4] and the particle diameter was 60 Å. All the samples here were prepared by dip coating Au foils from a concentrated colloidal solution. These foils were attached to a steel sample holder and loaded into the experimental chamber. At no stage during the experiments was sample charging observed.

3 Results and discussion

3.1 Pure SnO_2 nanoparticles

In the first instance we have investigated pure SnO_2 nanoparticles with the aim of understanding the surface chemical bonding. As the particles were exposed to air we wished to ascertain the extent of surface oxidation or structural disorder. Figure 1a shows an O 1s core level spectrum fitted with two Voigt components. With increasing photon energy and therefore increasing sampling depth, the intensity ratio of the two components changes as shown in Figure 1b. We see that the component on the low kinetic energy side of the spectrum is due to O atoms in a surface environment.

With respect to the bulk component, the surface component has a binding energy shift of $+1.30 \pm 0.05$ eV, which is the same shift found for surface hydroxyl groups (OH^-) in a study of thin film SnO_2 [7]. We suggest that the surface hydroxyl groups bond to the surface in a manner similar to that found for the O bridging atoms (O^{2-}) of the SnO_2 (110) surface [8].

The valence band spectrum of Figure 1c is consistent with an oxygen rich surface in that the peak closest to the valence band maximum (VBM) which is associated with O 2p valence electrons is reduced in intensity at higher photon energies (not shown). The surface described so far implies that there is no surface environment for Sn atoms, evidence for which is now discussed.

There are three main peaks before the VBM of Figure 1c. There is a weak tailing-off into the band gap above the VBM but we cannot confirm the existence of a surface state, *i.e.* a well defined peak in the band gap. Such a surface state would confirm the presence of surface Sn atoms in the form of four-fold coordinated Sn^{2+} [9]. Even though the valence band spectrum of Figure 1c was not recorded with maximum surface sensitivity (*i.e.* $h\nu =$ 766.25 eV), our evidence against the presence of a Sn surface state holds as these, if present, are detectable in tin oxides even in spectra recorded with $h\nu = 1486.6$ eV [9].

It would appear that there is no clear surface environment for Sn. We confirm this by the fact that the Sn 3d core level spectrum is fitted successfully with one Voigt function only (Figure 1d). Therefore Sn is involved in bulk chemical bonds only and its valence state is Sn^{IV} throughout the nanoparticles.

Here we have shown that there is a bulk and surface chemical environment for oxygen atoms but Sn is confined to the interior or bulk in this system. We are also sure that the surface has a well defined crystal structure because of the three well separated valence band peaks . This would not be the case if random oxide structures with excessive disorder were present at the surface [9].

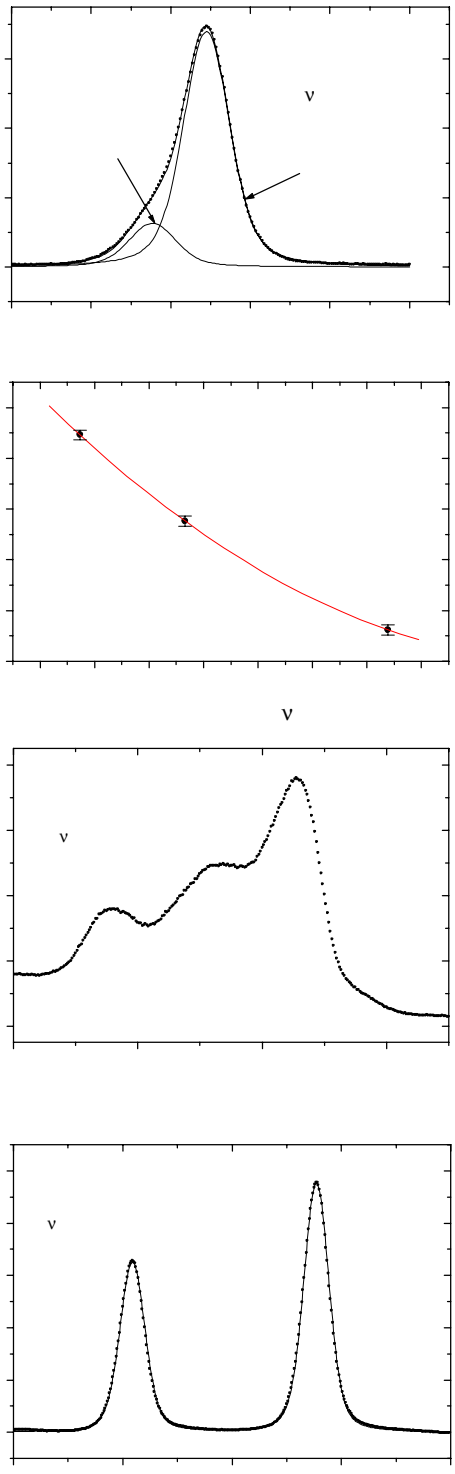

Fig. 1. Photoemission data for pure SnO_2 nanoparticles. (a) O 1s core level spectrum fitted with two Voigt components. (b) Intensity ratio of the components in (a) as a function of the photon energy. Valence band spectra are consistent with an oxygen rich surface (c) while the Sn 3d core level is fitted with one Voigt function only (d).

3.2 Sb doped SnO_2 nanoparticles

The controlled doping of semiconductor nanoparticles is an interesting challenge, see Ref. [3] for example. For SnO_2 nanoparticles, successful n-type doping with Sb

[6,4,10] leads to the question of how Sb is distributed in the nanoparticles and whether or not the Sb oxidation state is similar throughout the structure. Again using the sampling depth control available with tunable synchrotron radiation we have measured the Sb:Sn core level intensity ratio from progressively deeper regions of the nanoparticle layers. The maximum electron escape depth is approx. 25 Å.

Figure 2 shows this data for samples prepared with Sb concentrations of 9.1% and 16.7% while the inset shows one of the wide range photoelectron spectra from which the data points were evaluated. Here peak intensity refers to the area under the Sb $3d_{3/2}$ or Sn $3d_{3/2}$ photoemission peaks. Intensities were normalised to the photoionisation cross-section at each photon energy with data taken from Ref. [11]. Normalisation to light intensity was ignored as we assume constant light flux in the 5 second interval between the recording of the Sb 3d and Sn 3d spectra at any given photon energy. Data points also include a correction for the energy dependent sensitivity of the analyser which was taken from Ref. [12]. This was necessary because of the 45 eV kinetic energy difference between photoelectrons from the two levels at any photon energy. Figure 2 shows that there is an enrichment of Sb at the surface in SnO_2 nanoparticles doped with either 9.1% or 16.7% Sb.

Controlled doping of semiconductor nanoparticles is important for the manipulation of their optical and electronic properties. We show in Figure 2 that Sb is incorporated throughout the nanoparticles and it remains below to determine its oxidation state so as to clarify the origin of the n-type doping.

Two sample types were prepared by using either Sb^{III} or Sb^{V} as the chemical precursor in the reaction process. All samples were annealed to 500 °C to induce n-type conductivity. We aim to establish the valence state of the Sb atoms in the samples. In Figure 3a we show a fitted Sb $3d_{3/2}$ core level spectrum recorded from a sample prepared with Sb^{III} as the precursor. The binding energy scale was evaluated relative to the Fermi level of gold. We also compare the binding energy of the primary component with the Sb $3d_{3/2}$ binding energies found for samples of Sb_2O_3 and Sb_2O_5 [13]. The point here is that Sb is in the state Sb^{III} and Sb^{V} in these two oxides respectively. This simple comparison allows us to determine whether we have Sb^{3+} or Sb^{5+} ions in these particles. Figure 3a shows that for SnO_2 samples prepared with an Sb^{III} precursor, the predominant oxidation state is close to Sb^{V}. A similar reasoning was used in determining the nature of Sb in an analog of cubic perovskites [14]. There is a shift in binding energy between our measured spectrum and that of Sb $3d_{3/2}$ in Sb_2O_5 which is due to the chemical shift, *i.e.* a change in the Madelung energy associated with the two different crystal lattice types [15]. For samples prepared with Sb^{V}, the Sb 3d core levels have the same binding energy as that shown in Figure 3a so we may conclude that the final oxidation state of Sb in SnO_2 is the same for either precursor.

A low kinetic energy component is needed to fit the Sb $3d_{3/2}$ data of Figure 3a. Necessity for the second component is not clearly visible in the raw data in contrast to the O 1s data of Figure 1a but the data cannot be consistently fitted over a range of photon energies without two components. The photon energy dependence of the intensity ratio of these core level components is plotted in Figure 3b. A clear trend is that the peak to lower kinetic energy is enhanced in relative intensity when we increase the sampling depth at higher photon energies. This situation is typical for the situation where extrinsic plasmons are created by the longitudinal electric field of the outgoing photoelectron. Such an energy loss process occurs in material with a high concentration of conduction band electrons and in this case the loss feature is due purely to excitation of the conduction band electrons only. Enhancement of this process with increasing photon energy is typical for extrinsic plasmons [16]. Intrinsic plasmons, where it is the photohole remaining after photoemission

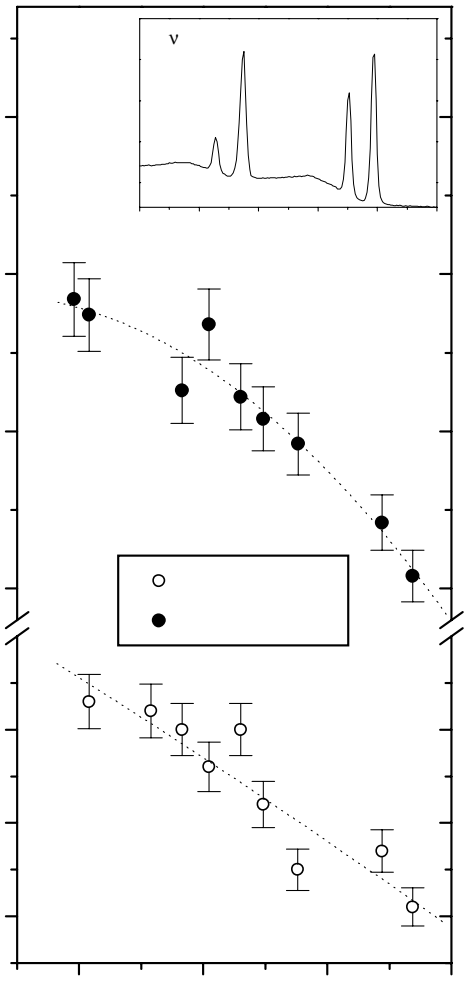

Fig. 2. Sb:Sn $3d_{3/2}$ core level intensity ratio as a function of photon energy for samples with two different Sb concentrations. Lines are drawn to guide the eye. The inset shows a typical wide range spectrum from which the core level intensities were calculated.

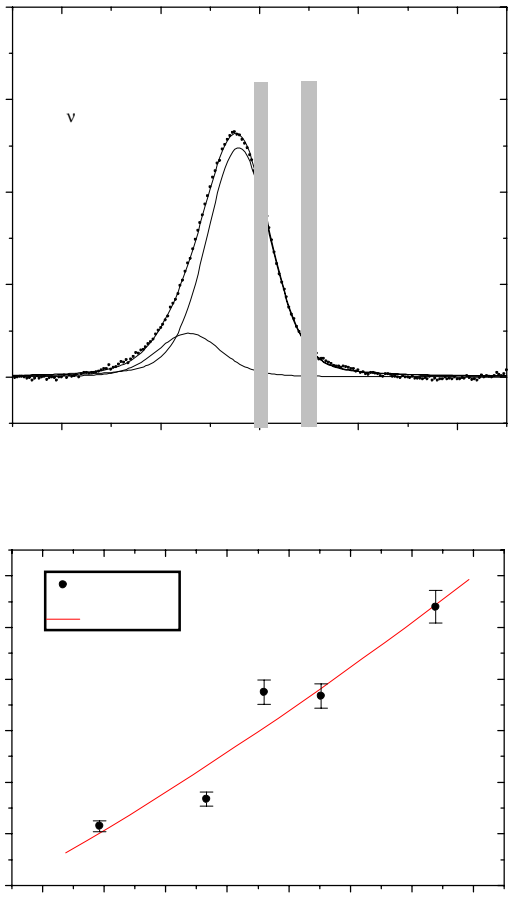

Fig. 3. Sb $3d_{3/2}$ core level fitted with two Voigt functions (a). Intensity ratio of the components in (a) as a function of photon energy (b) where the data are fitted to a polynomial function.

which excites the conduction band electrons are also possible although these are not expected to have a sampling depth intensity dependence as in Figure 3b.

Loss features are also observed for SnO_2 thin films doped with 3% Sb [17] but the plasmon satellite lines had a much higher intensity than we observe here. This disparity may be due to internal surfaces and boundaries in the nanoparticles because proximity of a surface has been shown to reduce the intensity of electron-bulk plasmon coupling [18]. Internal surfaces such as crystallographic shearing planes and twin boundaries are prevalent in nanocrystalline pure SnO_2 thin films [19]. The presence of such defects in our samples may therefore account for the weak intensity of the satellite feature of Figure 3a as well as the large surface environment in general and also electron confinement effects as discussed in Refs. [5,6].

4 Summary and conclusions

We have shown that pure SnO_2 nanoparticles with a diameter of 60 Å are terminated by an oxygen rich surface containing hydroxyl groups. Experimental results also suggest no surface environment for Sn atoms. We emphasize that these nanoparticle layers are suitable for studying by synchrotron radiation techniques as their surface quality remains high despite exposure to air and there is no evidence for sample charging during photoemission.

Photoemission features are however very broad with a Gaussian FWHM of 1 eV when the total experimental resolution was set to 240 meV. This highlights the effect of the expected internal faceting on photoemission core levels.

Nanoparticle layers which were doped n-type with 9.7% or 16.7% Sb have dopant atoms concentrated at the surface whose oxidation state is predominantly Sb^V. Further work in comparing valence band and Sn 3d core level spectra in pure and n-type doped nanoparticle layers will establish the characteristics of electron occupation in doped nanoparticles.

References

1. H. Weller, Adv. Mat. **5**, 88 (1993).
2. A.P. Alivisatos, Science **271**, 933 (1996).
3. M. Shim, P. Guyot-Sionnest, Nature **407**, 981 (2000).
4. J. Rockenberger, U. zum Felde, M. Tischer, L. Tröger, M. Haase, H. Weller, J. Chem. Phys. **112**, 4296 (2000).
5. U. zum Felde, M. Haase, H. Weller, J. Phys. Chem. B **104**, 9388 (2000).
6. G. Boschloo, D. Fitzmaurice, J. Phys. Chem. **103**, 3093 (1999).
7. G. Gaggiotti, A. Galdikas, S. Kačiulis, G. Mattogno, A. Šetkus, J. Appl. Phys. **76**, 4467 (1994).
8. T.J. Godin, J.P. LaFemina, Phys. Rev. B **47**, 6518 (1993).
9. J.M. Themlin, M. Chtaib, L. Henrard, P. Lambin, J. Darville, J.M. Gilles, Phys. Rev. B **46**, 2460 (1992).
10. T. Nütz, U. zum Felde, M. Haase, J. Chem. Phys. **110**, 12142 (1999).
11. J.-J. Yeh, *Atomic Calculation of Photoionization Cross-Sections and Asymmetrey Parameters* (Gordon and Breach, Berlin, 1993).
12. P. Ruffieux, P. Schwaller, O. Gröning, L. Schlapbach, P. Gröning, Q.C. Herd, D. Funnemann, J. Westermann, Rev. Sci. Instrum. **71**, 3634 (2000).
13. C.D. Wagner, *Handbook of Photoelectron Spectroscopy* (Perkin Elmer, Eden Prairie, MN, 1979).
14. R. Claessen, M.G. Smith, J.B. Goodenough, J.W. Allen, Phys. Rev. B **47**, 1788 (1993).
15. W. Mönch, *Semiconductor Surfaces and Interfaces* (Springer-Verlag, Berlin, 1993).
16. S.A. Flodstrom, R.Z. Bachrach, R.S. Bauer, J.C. McMenamin, S.B.M. Hagström, J. Vac. Sci. Technol. **14**, 303 (1977).
17. R.G. Egdell, J. Rebane, T.J. Walker, D.S.L. Law, Phys. Rev. B **59**, 1792 (1999).
18. J.J. Chang, D.C. Langreth, Phys. Rev. B **8**, 4638 (1973).
19. X. Pan, J.G. Zheng, Mat. Res. Soc. Symp. Proc. **472**, 87 (1997).